Combustion Science and Technology
Publication details, including instructions for authors and subscription information:
http://www.tandfonline.com/loi/gcst20

EFFECT OF OPPOSED FLOW ON FLAME SPREAD OVER A FINITE-LENGTH PMMA SLAB IN A TWO-DIMENSIONAL WIND TUNNEL

WEN-KUEI CHANG [a] & CHIUN-HSUN CHEN [a]
[a] Department of Mechanical Engineering , National Chiao-Tung University , HsinChu, Taiwan, R.O.C.
Published online: 22 Oct 2007.

To cite this article: WEN-KUEI CHANG & CHIUN-HSUN CHEN (2007) EFFECT OF OPPOSED FLOW ON FLAME SPREAD OVER A FINITE-LENGTH PMMA SLAB IN A TWO-DIMENSIONAL WIND TUNNEL, Combustion Science and Technology, 179:12, 2489-2510, DOI: 10.1080/00102200701484316

To link to this article: http://dx.doi.org/10.1080/00102200701484316

Combust. Sci. and Tech., 179: 2489–2510, 2007

ISSN: 0010-2202 print/1563-521X online
DOI: 10.1080/00102200701484316

Taylor & Francis
Taylor & Francis Group

Effect of Opposed Flow on Flame Spread over a Finite-Length PMMA Slab in a Two-Dimensional Wind Tunnel

Wen-Kuei Chang and Chiun-Hsun Chen
Department of Mechanical Engineering, National Chiao-Tung University, HsinChu, Taiwan, R.O.C.

Abstract: The ignition delay and subsequent downward flame spread over a finite-length PMMA slab with the effect of radiation included in a two-dimensional wind tunnel are investigated using the opposed flow velocity as a parameter. The gas and solid phase temperatures, preheat length and heat flux are considered in order to examine the flame ignition and spread characteristics. The numerical results reveal that the ignition delay time increases with the opposed flow velocity. However, the flame spread rate varies with the opposed flow velocity in a non-monotonic manner that can be identified as two distinct regimes with a peak value in between. The flame spread rate reaches a maximum at $V_g = 32\,\mathrm{cm/s}$, and then falls, regardless of whether the flow velocity is increasing or decreasing. For $V_g < 32\,\mathrm{cm/s}$, the flame behaviors are dominated by oxygen transport. For $V_g > 32\,\mathrm{cm/s}$, the flame stretch effect controls the flame behavior. Additionally, this work demonstrates that the effect of radiation delays the flame ignition and reduces both the flame strength and the corresponding spread rate. The effects of the opposed flow temperature and thickness of the solid fuel are also investigated. The predicted results indicate that a higher opposed flow temperature or a thinner solid fuel facilitates the ignition and accelerates flame spread. The effect of opposed flow velocity eventually overcomes that of opposed flow temperature as the flow speed is further increased.

Received 22 December 2006; accepted 27 April 2007.
The authors would like to thank the National Science Council of the Republic of China, Taiwan, for financially supporting this research under Contract No. NSC 95-2625-Z-009-003.
*Address correspondence to chchen@mail.nctu.edu.tw

Keywords: Downward flame spread; Ignition delay; Opposed flow velocity; Radiation effect

INTRODUCTION

This work investigates flame ignition and the characteristics of the subsequent flame spread over a finite-length PMMA slab in an opposed convection environment in a two-dimensional wind tunnel, using an unsteady combustion model that incorporates both gas and solid phase radiation. Pan (1999) and Chen (1999) performed the corresponding experiments using the opposed gas flow velocity and temperature, and the solid fuel thickness as parameters. They found that the flame spread rate increases with the flow temperature, a drop in the flow velocity or a decline in the thickness of the fuel. Their results further indicated that the thermal boundary layer becomes thicker as the opposed flow temperature increases at a fixed flow velocity or as the opposed flow velocity declines at a constant flow temperature.

The flame spread rates predicted by Wu et al. (2003) were compared with the measurements made by Pan (1999). They were highly consistent, except in the slow flow regime. The differences between the predicted results and the experimental measurements are believed to be attributable to several factors, such as the fuel length and radiation in the gas and solid phases, which were not under consideration in their investigation. Chang et al. (2006) made an intensive modification according to the aspects mentioned above to mitigate the discrepancies between the predictions and the measurements. The comparison produced simulated results that were more similar to the experimental values. They demonstrated that the fuel length and the inclusion of solid phase radiation significantly affected the ignition delay time and flame spread rate. However, gas phase radiation can be neglected because the flame spreads in a high speed flow regime.

Several investigations, such as those of West et al. (1994), Bhattacharjee and Altenkirch (1991) and Bhattacharjee et al. (2000), found that radiation from the fuel surface is important at any flow velocity, when the fuel is thermally thick, and the flame spread rate and the temperature drop as the solid surface emittance is increased. Rhatigan et al. (1998) examined the effects of gas phase radiation on the burning and extinction of a solid fuel. They plotted the heat fluxes, flame temperature and burning rate as functions of the flow stretch rate. The computed results demonstrated that the gas phase radiative effects are stronger at lower stretch rates. Fernandez-Pello and Hirano (1982) experimentally studied the controlling mechanism of flame spread over the surface of combustible solids. The heat transfer and gas phase

chemical kinetic aspects of the flame spread process were addressed respectively for the flame spread in oxidizing flow. They indicated that chemical kinetics of gas phase plays a critical role and it must be considered when flame spread in opposed gas flow occurs at near extinction or non-propagating conditions.

Son and Ronney (2002) experimentally studied flame spread over thermally thick fuels. They found that the radiative preheating and reabsorption effect are less important in normal gravity, because a substantial flow velocity is caused by buoyancy, reducing the thickness of the flame and thereby reducing the volume of radiating gas. Takahashi et al. (2000) and Ayani et al. (2006) examined flame spread rates over PMMA sheets in normal gravity and in microgravity. They found that the flame spread rate over a thermally thin fuel is inversely proportional to the thickness of the fuel, whereas that over a thermally thick fuel is proportional to the opposed flow velocity, in complete agreement with analyzed research by DiRis (1969). Other investigations, such as Wichman and Williams (1983a), Wichman and Williams (1983b) and Delichatsios (1986), have developed formulas that show identical proportionalities. The angle of the pyrolysis region remains roughly constant as the sheet thickness is varied.

Tizon et al. (1999) analyzed the wind-aided flame spread process along a solid fuel rod under oblique forced flow. Their results indicated that the effects of gas-phase chemical kinetics were important for large strain rates and the spread rate depended strongly on the strain rate. They also found that the effects of radiation from the gas phase are negligible because the heat transfer by convection typically dominates at large Reynolds numbers of the transverse velocity. Fujita et al. (2002) experimentally investigated the effect of external flow on flame spread over polyethylene wires in microgravity. The results revealed that the flame spread rate is controlled mainly by preheat length, standoff distance and flame temperature. The flame spread phenomenon can be divided into three regimes based on flow velocity. These are an oxygen transport control regime, a geometrical effect regime and a chemical-kinetics controlled regime.

Wichman (1983) developed a theoretical model to estimate the rate of flame spread under conditions of heat transfer control with account taken of the fact that the gas velocity was not uniform. The results indicated that the functional dependence of the spread rate on the external gas velocity is modified from the one obtained in the classical study of DeRis (1968). Thereafter, Wichman (1992) explained two mechanisms for the extinguishment of spreading flames. In the first, the particle residence time in the reaction zone is reduced by the increased flow velocity, giving a blow off extinction. In the second, flow velocity decreases toward flame spread rate and extinction again occurs eventually.

Takahashi et al. (2002) analytically and experimentally studied flame spread over a thin PMMA sheet in microgravity. They concluded that reducing the relative flow velocity enlarges the size of preheat zone, increasing radiant loss, and that radiant heat loss reduces the flame spread rate and may also cause extinction.

The aforementioned series of studies, such as those of Pan (1999), Wu et al. (2003) and Chang et al. (2006), concluded that the influence of opposed flow velocity on the flame spread behavior exceeds that of opposed flow temperature as flow velocity is increased further, and that the discrepancies between the predicted and measured results, especially in the low flow speed regime are due to the radiation effect. Moreover, numerous investigations, such as those of West et al. (1994), Rhatigan et al. (1998), Tizon et al. (1999) and Zhu and Gore (2005), demonstrated that the radiation effect becomes stronger as the flow speed declines. Therefore, this work systematically investigates the effects of opposed flow velocity on the flame spread characteristics considering the radiation effect over a thick solid fuel of finite length in a two-dimensional wind tunnel. The opposed flow velocities simulated herein are varied from 0 to 100 cm/s, whereas the ones used by Pan (1999), Wu et al. (2003) and Chang et al. (2006) are varied from 40 to 100 cm/s. The entire process, from ignition to subsequent flame spread, is examined in detail. The effects of opposed flow temperature, solid fuel thickness and radiation heat loss at various flow velocities are also discussed. Finally, possible extensions of this work are suggested.

MATHEMATICAL MODEL

Figure 1 presents the physical configuration of two-dimensional ignition over a vertically oriented PMMA sample in a mixed convective environment. The test section of the wind tunnel is 70 cm long and 10 cm high. The solid fuel plates used in the simulation are 30 cm long and 0.82 cm and 1.74 cm thick. The solid fuel is assumed to be homogeneous, meaning that its composition is uniform. At $t < 0$, a steady flow in the wind tunnel builds up over the entire test section. In the channel flow the surface velocity gradient is given by $a = 4V_g/H$, where V_g is the centerline flow velocity and H the height of the wind tunnel. At $t \geq 0$, an external heat flux with a Gaussian distribution with a width of 0.5 cm and a peak value of 5 W/cm^2, is imposed on the solid fuel surface and centered at $x = 0$, where the top end of the solid fuel is connected to an adiabatic plate. Restated, only half of the incident radiation energy is used to heat the PMMA fuel. The solid fuel absorbs the external heat flux to raise its temperature gradually. Then, the solid fuel begins to pyrolyze and generate fuel vapors, which mix with air to form the flammable mixture

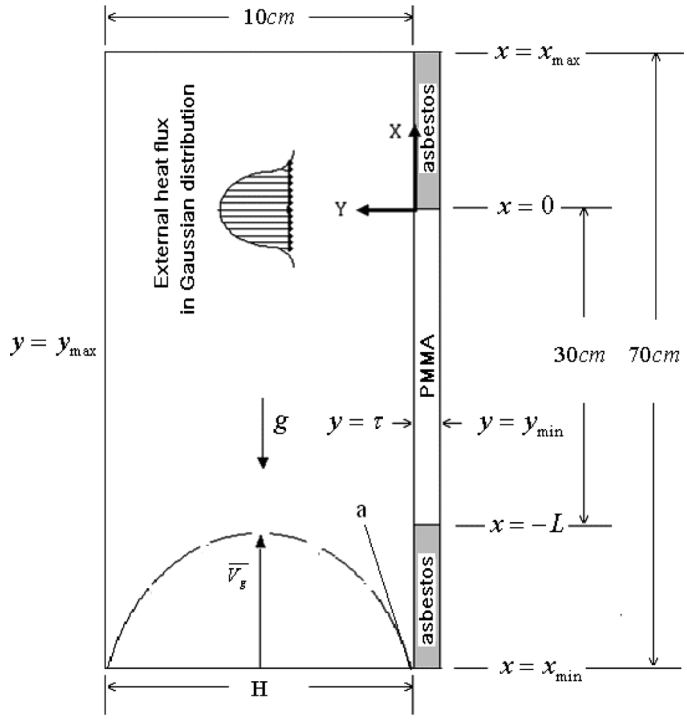

Figure 1. Physical configuration of two-dimensional ignition over a vertically oriented PMMA sample in a mixed convective environment.

adjacent to the surface of the fuel. Ignition occurs when the gas phase temperature is high enough to promote the chemical reaction. Subsequently, the flame begins to propagate, eventually reaching a steady rate of spread.

The unsteady combustion model and radiation model are basically modified from those developed by Lin and Chen (2000) and Wu and Chen (2004). However, Wu and Chen (2004) applied the P1 radiation model, in which the semi-gray scheme is adopted to define the effective absorption coefficient. Since the gas phase radiative properties depend strongly on the temperature and mixture concentrations, the simple assumptions used in these prior simulations are unrealistic and unsuitable for determining the radiative properties. Therefore, this work modifies the model of Wu and Chen (2004) by using the narrow band model instead of the P1 model to calculate the gas phase absorption coefficient and the radiation intensity. In this problem, the mathematical model consists of both gas and solid phase equations, which are coupled at the

interface. The assumptions regarding radiation in gas and solid phases are as follows:

1. Gas phase radiation is 2D. The narrow band model is employed to determine the radiation heat flux.
2. The gas is optically thin and the scattering effect is neglected because the production of soot is not considered in the gas phase chemical reaction.
3. The participating media are CO_2 and H_2O.
4. Soot radiation and surface reflectivity are neglected.
5. The fuel surface is opaque and diffuse.

The gas phase energy equation is

$$\bar{\rho}\bar{C}_p\frac{\partial\overline{T}}{\partial\bar{t}}+\bar{\rho}\bar{C}_p\bar{u}\frac{\partial\overline{T}}{\partial\bar{x}}+\bar{\rho}\bar{C}_p\bar{v}\frac{\partial\overline{T}}{\partial\bar{y}}=\frac{\partial}{\partial\bar{x}}\left[\bar{k}\frac{\partial\overline{T}}{\partial\bar{x}}\right]+\frac{\partial}{\partial\bar{y}}\left[\bar{k}\frac{\partial\overline{T}}{\partial\bar{y}}\right]-\bar{q}\bar{\dot{\omega}}_F-\nabla\cdot\bar{q}^r \tag{1}$$

where $\nabla\cdot\bar{q}^r=(\partial\bar{q}^r_x/\partial\bar{x})+(\partial\bar{q}^r_y/\partial\bar{y})$ is the gas phase radiation term.

For the forced convection channel flow, the radiation terms $\partial\bar{q}^r_x/\partial\bar{x}$ and $\partial\bar{q}^r_y/\partial\bar{y}$ can be expressed as (Siegel and Howell, 1992):

$$\nabla\cdot\bar{q}^r=\frac{\partial\bar{q}^r_x}{\partial\bar{x}}+\frac{\partial\bar{q}^r_y}{\partial\bar{y}}=8\pi\bar{a}(\bar{I}_b-\bar{I}) \tag{2}$$

in which $\bar{I}_b$ represents the blackbody intensity, $\sigma\overline{T}^4/\pi$, and $\overline{I}$ is the radiation intensity.

At the interface of the gas phase and the solid fuel surface, the boundary condition is

$$\bar{k}_s\frac{\partial\overline{T_s}}{\partial\bar{y}}=\bar{\mu}\frac{\partial\overline{T}}{\partial\bar{y}}+\bar{q}_{ex}-\frac{\varepsilon\sigma}{\bar{\tau}}\left(\overline{T_s}^4-\overline{T}_\infty{}^4\right)+\frac{\overline{q}^r_y}{\bar{\tau}} \tag{3}$$

where $-\frac{\varepsilon\sigma}{\bar{\tau}}\left(\overline{T_s}^4-\overline{T}_\infty{}^4\right)$ and $\overline{q}^r_y/\bar{\tau}$ are heat lost by radiation from solid to ambient gas and radiation feedback from gas to solid, respectively. Details of the governing equations and assumptions can be found in Wu et al. (2003) and are not repeated here.

This two-dimensional numerical study is conducted using the opposed flow velocity as a parameter to investigate flame ignition and the subsequent downward flame spread behavior. This work also discusses the effects of the opposed flow temperature and the solid fuel thickness. Notably, in the present simulation, a finite-length fuel slab is used, the ignition/combustion is in a two-dimensional wind tunnel, and both gas and solid phase radiation is considered. The ambient pressure and the ambient oxygen concentration in this model are fixed at 1 atm

Table 1. Gas and solid properties values

Symbol	Value	Unit
$\overline{E}_s$	1.298×10^5	J/mol
$\overline{A}_s$	2.282×10^9	1/s
$\overline{L}$	-941.08	J/g
$\overline{k}_s$	2.675×10^{-3}	W/cm K
$\overline{C}_s$	1.465	J/gK
$\overline{\rho}_{s\infty}$	1.19	g/cm^3
$\overline{T}_v$	668	K
f	1.92	—
$\overline{C}_p$	$f(\overline{T}^*)$	J/g K
$\overline{u}_\infty$	variable	Cm/s
$Y_{O\infty}$	0.233	—
$\overline{\rho}^*$	$f(\overline{T}^*)$	g/cm^3
$\overline{q}$	2.59×10^4	J/g
$\overline{\alpha}^*$	$f(\overline{T}^*)$	cm^2/s
$\overline{T}_\infty$	variable	K
$\overline{k}^*$	$f(\overline{T}^*)$	W/cm K
$\overline{\mu}^*$	$f(\overline{T}^*)$	g/cms
$\overline{E}$	8.895×10^4	J/mol
$\overline{B}$	5.928×10^{12}	cm^3/mols
$\overline{\tau}$	variable	cm
ε	1	—

and 0.233, respectively. Table 1 presents the physical data used in this work.

The numerical scheme utilizes the SIMPLE algorithm developed by Patankar (1980). The present radiation model incorporates the subroutine RADCAL developed by Grosshandler (1993) to determine the absorption coefficient. Since the radiation subroutine is complicated and consumes much computing time, it is executed once after 10 iterations in each time step. The unsteady governing equations are solved subject to the interface and boundary conditions in each time step until a convergence criterion (residual < 0.01) is satisfied. Thereafter, the procedure moves to the next time step. Computations are carried out using a non-uniform mesh distribution. The smallest grid is 0.01 cm wide. Most of the grid points are clustered in an external radiative heating region to capture drastic variations in the flame. The grids expand upstream and downstream. According to the grid-independence test, a non-dimensional time step of $\Delta t = 10$ (equivalent to a real time of 0.02 s) and non-uniform grid dimensions of 290×95 were found to optimize the balance among resolution, computational time and memory space requirements. The time step that was selected in this work is much smaller than those

used in previous studies, such as 0.0548 s in Lin and Chen (2000) and 0.05 s in Wu and Chen (2004). Hence, the present computation is expected to be more accurate and suitable for examining gas phase ignition. The computational time associated with each case was approximately 2 days on a 2.8 GHz Intel Pentium 4 PC at National Chiao Tung University.

RESULTS AND DISCUSSION

Figure 2 plots the computed ignition delay time as a function of opposed flow velocity at a fixed opposed flow temperature of 313 K with and without radiation in the gas and solid phases. The ignition delay time is defined herein as the instant at which the first appearance of the dimensional reaction rate reaches $10^{-4}\,g/cm^3\,s$. This figure reveals that the ignition delay time increases with the opposed flow velocity. This occurs because the temperature of the solid fuel increases to the pyrolysis temperature with greater difficulty in the faster flow due to the stronger convective cooling effect. In addition, most of the generated fuel vapors are carried downstream by the fast flow, extending the formation time of a flammable mixture adjacent to the solid fuel surface. Therefore, for these two reasons the ignition delay time is longer in the faster flow regime. Furthermore, in Figure 2 the results with and without the effect of radiation are compared. The ignition delay with radiation is expected to be

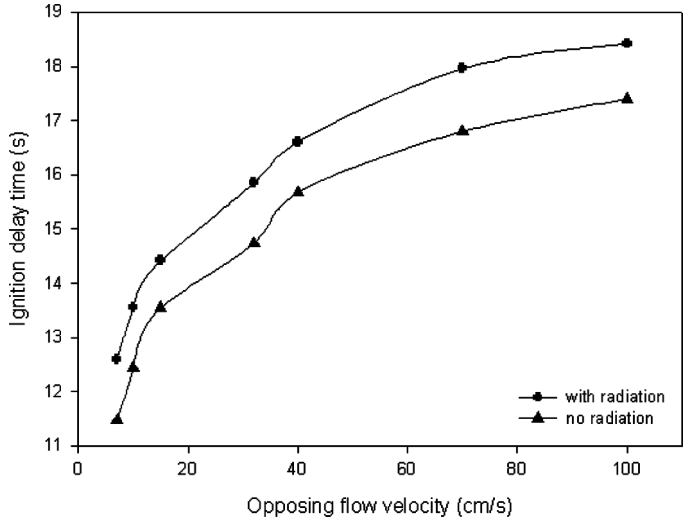

Figure 2. Ignition delay times as functions of opposed flow velocity at a fixed opposed flow temperature of 313 K with and without radiation.

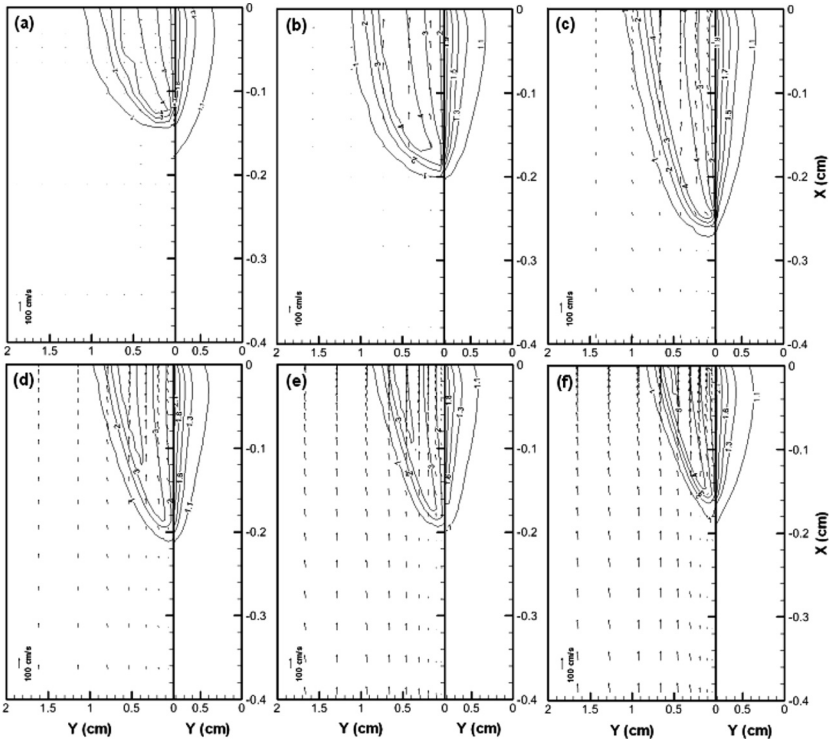

Figure 3. Flow velocity vector distributions and non-dimensional temperature contours for gas and solid phases at various opposed flow velocities, (a) 7 cm/s, (b) 15 cm/s, (c) 32 cm/s, (d) 40 cm/s, (e) 70 cm/s and (f) 100 cm/s, at a fixed opposed flow temperature of 313 K. The centerline of wind tunnel is at 5 cm along the Y axis of the left-hand side (not display in the figure).

longer than that without radiation. The solid fuel requires more time and energy to reach the pyrolysis temperature in order to produce fuel vapors as heat is lost by radiation, these increasing the formation time of the flammable mixture and the ignition delay time as well. In the ignition stage radiant loss therefore dominates radiant heat absorption by the gas and the sold.

Figure 3 plots the flow velocity vector distributions and the non-dimensional temperature contours for the gas and solid phases at several opposed flow velocities at a fixed opposed flow temperature of 313 K. Notably, both gas and solid phase radiation is considered. The left and right-hand sides of Figure 3 depict the temperature contours for the gas and solid phases, respectively. Both fronts of temperature contours (gas and solid phase) along the solid fuel surface move further upstream (the upstream defined herein is the direction of inlet opposed flow) and

then shift back to downstream as the opposed flow velocity continuously increases. Additionally, the flame size is reduced and the gas temperature contours are pushed toward the solid fuel surface as the opposed flow velocity increases. Also, the curvature of the apex of the temperature contours declines as the opposed flow velocity increases. In this figure, it can be found that some of the flames are further upstream than others. This is because the flame spread rate varies with the opposed flow velocity non-monotonically. The faster flame spread rate leads to the flame further upstream. These aforementioned phenomena will be discussed in detail later.

Figure 4 plots the fuel and oxidizer mass fraction distributions that correspond to Figure 3. The solid and dashed lines represent the fuel and oxidizer mass fraction distributions, respectively. Clearly, the fuel and oxidizer are premixed well at the flame front. The premixed flammable mixture plays the role of a source to support combustion enabling the flame can therefore sustain itself to spread upstream. This fact that there is premixing near the flame leading edge was first noted in the PhD thesis of DeRis (1968) and subsequently a detailed discussion was given by Wichman and Osman (1998). Behind the premixed region, the flame is a diffusion flame.

Figure 5 plots the predicted flame spread rate as a function of opposed flow velocity at a fixed opposed flow temperature of 313 K with and without gas and solid phase radiation. The flame spread rate is determined by the motion of the pyrolysis front, which is defined as the first position of $\rho_s = 0.99$. The flame spread rate varies with the opposed flow velocity non-monotonically and two flame spread regimes are separated by the peak value in between. The peak occurs at a flow velocity of approximately 32 cm/s and the maximum change in flame spread rate is about 13.2%. In the first regime, $V_g < 32\,\text{cm/s}$, where the flame spread rate increases with the opposed flow velocity. In the second regime, $V_g > 32\,\text{cm/s}$, where the flame spread rate decreases as the opposed flow velocity increases, opposite to the trend in the first regime. In the first flame spread regime, the controlling mechanism of flame spread is oxygen transport.

The higher speed opposed flow supplies more oxygen to the flame, to mix with the fuel vapor, shortening the formation time of the flammable mixture near the solid fuel surface, and thus strengthening the flame and accelerating the spread. However, as the opposed flow velocity increases into the second regime, the controlling mechanism of the flame spread is chemical kinetics. As the opposed flow velocity increases, most of the fuel vapors are carried downstream. The gas residence time decreases and the chemical reaction does not have sufficient time to proceed to completion, reducing the ratio of the residence time of the mixture to the chemical time (i.e. the Damköhler number). These phenomena mentioned above

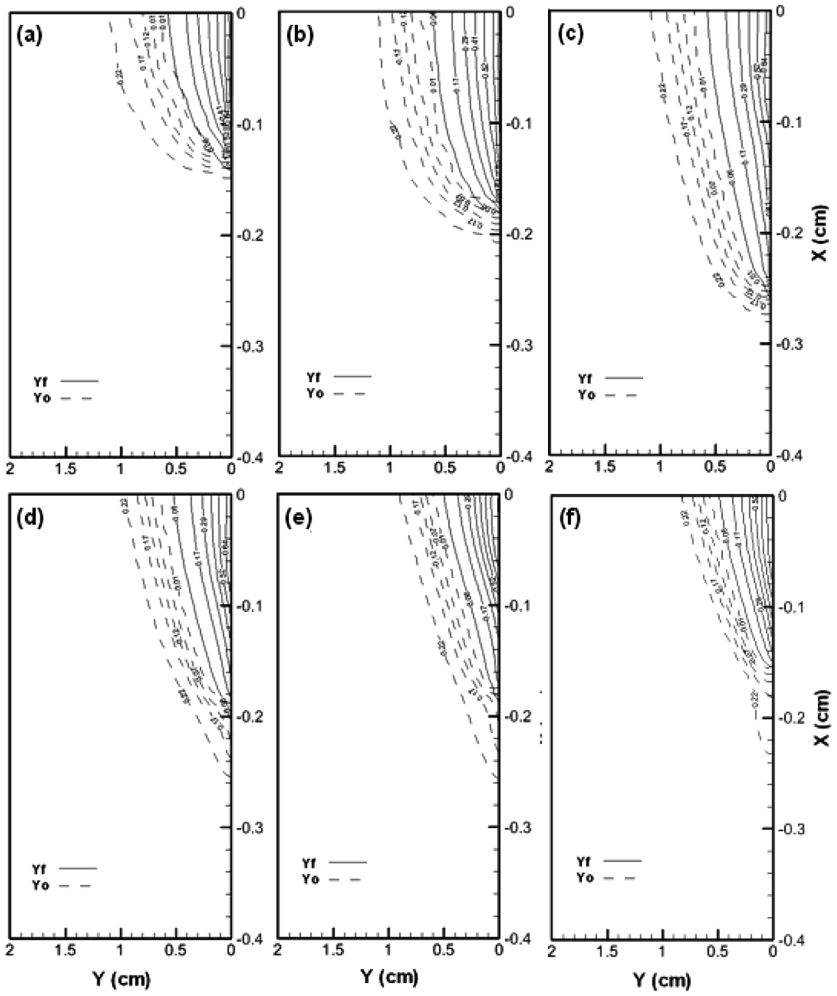

Figure 4. Fuel and oxidizer mass fraction distributions at various opposed flow velocities, (a) 7 cm/s, (b) 15 cm/s, (c) 32 cm/s, (d) 40 cm/s, (e) 70 cm/s and (f) 100 cm/s, at a fixed opposed flow temperature of 313 K.

have been confirmed by the prior study of DeRis (1968). In addition, the increase in the stretch effect reduces the thickness of the flame, as shown in Figure 3, and it is more difficult for the forward heat transfer from the flame to preheat the solid fuel. Consequently, the flame becomes weaker, such that the spread rate is lower in the regime of high flow velocity. Several numerical and experimental studies, such as those of Lastrina et al. (1971), Fernandez-Pello and Hirano (1982), Olson (1991), Wichman (1992), Tizon et al. (1999) and Fujita et al. (2002), have found this

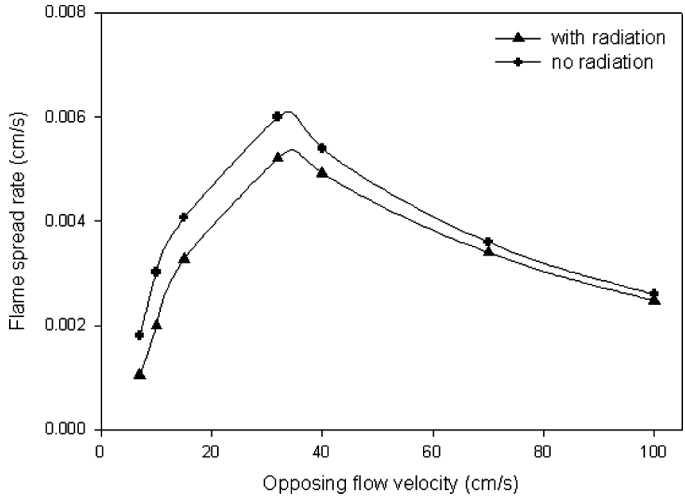

Figure 5. Flame spread rates versus opposed flow velocity at a fixed opposed flow temperature of 313 K with and without radiation.

qualitative trend of the flame spread rate mentioned above. Figure 5 reveals that the flame spread rates with radiation are all lower than those without radiation. The heat loss by radiation weakens the flame and reduces the spread rate as well. Figure 6 plots the heat flux magnitudes of q_{gr} and q_{sr} under various opposed flow velocities at a fixed opposed flow temperature of 313 K. The heat fluxes, q_{gr} and q_{sr}, represent the gas phase radiation feedback to the solid fuel and the heat loss by radiation from the solid fuel to the ambient, respectively.

The comparison of q_{gr} and q_{sr} demonstrates that the magnitude of the gas phase radiation is relatively much smaller, because the heat transfer mechanisms associated with flame spreading in a fast flow are dominated by conduction and convection. In other words, the maximum absolute values of q_{gr} and q_{sr} are 0.0499 and 0.812, respectively. Hence it can be found that $|q_{gr}|/|q_{sr}| << 1$. Accordingly, the apparent radiation heat transfer herein is preferentially only from the solid fuel to the ambient. Since q_{sr} is proportional to T_s^4 and the maximum solid fuel temperature herein is defined as the burnout temperature, 668 K, the magnitude of q_{sr} is almost invariant throughout the simulated flow speed regime.

A recirculation flow just ahead of the flame front is observed, and its intensity increases with the opposed flow velocity, as illustrated in Figure 7. This figure displays the temperature contours of the gas phase and the streamline distributions at a fixed opposed flow temperature of 313 K for the three opposed flow velocities of 7 cm/s, 32 cm/s and 100 cm/s. The presence of the recirculation flow enhances the mixing of

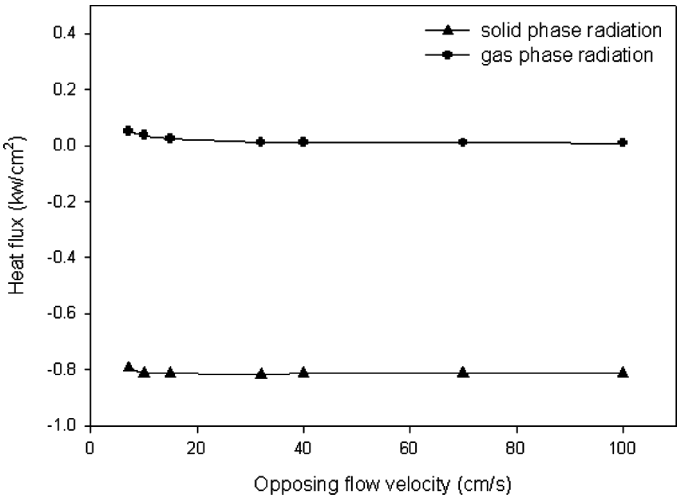

Figure 6. Heat flux magnitudes q_{gr} and q_{sr} at various opposed flow velocities at a fixed opposed flow temperature of 313 K. q_{gr} and q_{sr}, represent the gas phase radiation feedback to solid fuel and the radiation heat loss from the solid fuel to the ambient.

fuel vapor and the oxidizer. Additionally, the flow can also carry some heat upstream from the flame and simultaneously brings some of the cold air from upstream into the flame. These two mechanisms are competing with each other. As the flow velocity continues to increase, the latter effect outweighs the former one, indicating that the cooling effect is prominent. This phenomenon weakens the flame and reduces the corresponding spread rate. The recirculation region has been numerically confirmed by the prior researches, such as Whichman (1992) and Higuera et al. (1997).

Figure 8 plots the preheat lengths versus opposed flow velocity at a fixed opposed flow temperature of 313 K with and without radiations. The preheat length herein is defined as the distance between the non-dimensional temperature contours of 1.1 and 2.1 along the solid fuel surface, as shown in the inset of Figure 8. The maximum change in preheat length is about 15%. The preheat zone becomes narrower as the opposed flow velocity increases and the dependence on opposed flow velocity becomes stronger as the velocity declines. A larger preheat length corresponds to a shorter required time for solid fuel to raise its temperature to the pyrolysis temperature, thereby increasing pyrolysis intensity. However, an excessive preheat length causes the dispersion of heat across a rather wide region, slowing the flame spread, as displayed in Figures 5 and 8. These two figures demonstrate that the preheat length is larger

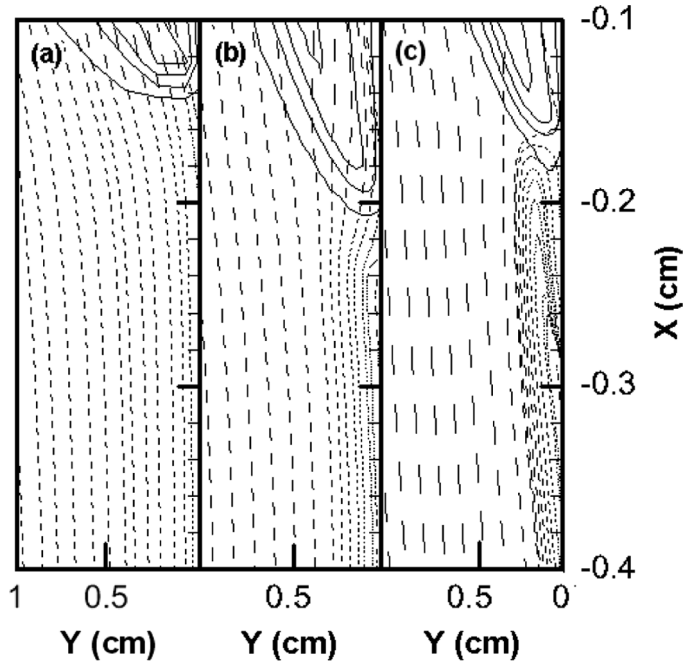

Figure 7. Temperature contour of gas phase and streamline distribution at a fixed opposed flow temperature of 313 K and opposed flow velocities of 7 cm/s, 32 cm/s and 100 cm/s.

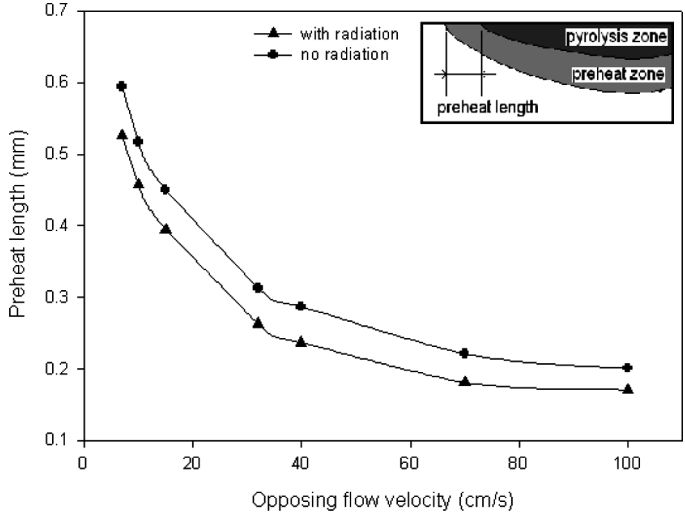

Figure 8. Preheat lengths versus opposed flow velocity at a fixed opposed flow temperature of 313 K with and without radiations.

in the region of lower flow velocity, but the corresponding flame spread rate is not higher. As the opposed flow velocity increases further, the convective cooling effect becomes stronger and the forward heat transfer from the flame to preheat the solid fuel becomes more difficult, shortening the preheat length. Furthermore, the preheat length with radiation is smaller than that without radiation because heat is lost by radiation, reducing the total heat received by the solid fuel.

Figure 9 plots the maximum flame temperature in the gas phase as a function of opposed flow velocity at a fixed opposed flow temperature of 313 K with and without radiation. The flame temperature initially increases sharply and then declines slightly as the opposed flow velocity increases, suggesting that the dependence on opposed flow velocity is stronger at lower velocity. According to the phenomena of flame spread mentioned previously, the variation of the flame temperature can also be divided into two regimes. In the first regime, prior to the flame spread rate maximum of Figure 5 where the opposed flow velocity is below 32 cm/s, the flame becomes stronger and the flame spread rate increases with the flow velocity, resulting in an increase of the flame temperature. In the second regime, where the opposed flow velocity exceeds 32 cm/s, the flame spread rate decreases as the opposed flow velocity increases, indicating that a weaker flame spreads in this flow velocity regime and, therefore, the flame temperature is reduced, but its variation is inconspicuous.

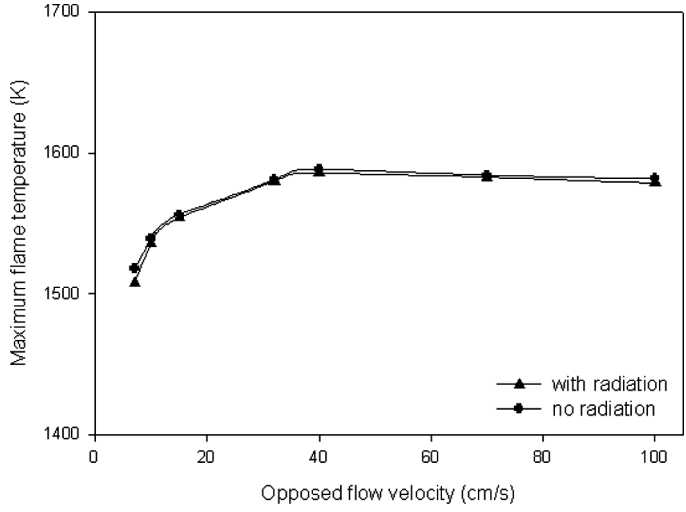

Figure 9. Maximum flame temperatures versus opposed flow velocity at a fixed opposed flow temperature of 313 K with and without radiation.

This result demonstrates that the effect of opposed flow velocity on the flame temperature in the high speed flow regime is not very significant, but it pushes the flame toward the solid fuel surface, allowing it to be more or less parallel to the surface, as shown in Figure 3. Pan (1999) and Chen (1999) also experimentally observed this phenomenon. Comparing the flame temperatures measured in these two experimental works (not shown here) reveals that the temperatures predicted herein are higher. This difference may possibly be attributed to the side heat loss from the flame to the side walls of the wind tunnel in the experiment. The wind tunnel utilized in the experimental test is three-dimensional, whereas the flame spreads in a two-dimensional wind tunnel in the present simulation. Note from Figure 9 that radiation only slightly affects the flame temperature because the magnitudes of the gas and solid phase radiation is small compared with the heat conducted in the gas phase.

Figure 10 plots the total heat fluxes received by the solid fuel against the opposed flow velocity at a fixed opposed flow temperature of 313 K with and without radiation. The maximum change in heat flux received by solid fuel is about 12%. From the previous figure, the variation of maximum flame temperature is quite insignificant, indicating that the solid-phase radiation makes more contribution in total heat flux than that of gas-phase one. The dependence of the heat supplied to the solid fuel on the opposed flow velocity can also be divided into two regimes,

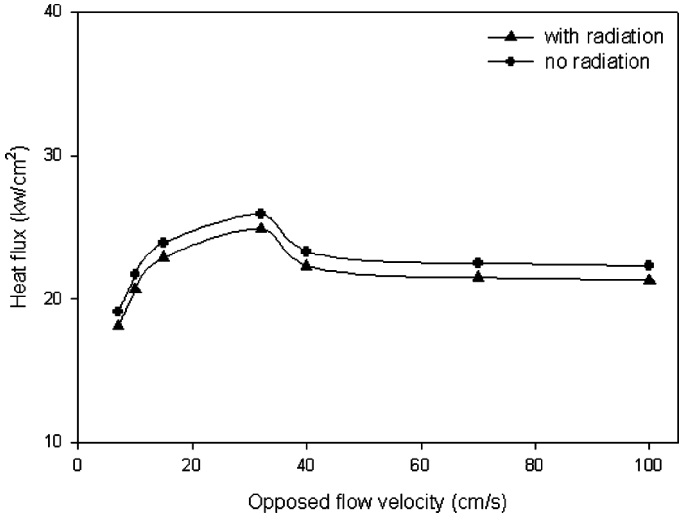

Figure 10. Total heat fluxes gained by solid fuel versus opposed flow velocity at a fixed opposed flow temperature of 313 K with and without radiations, respectively.

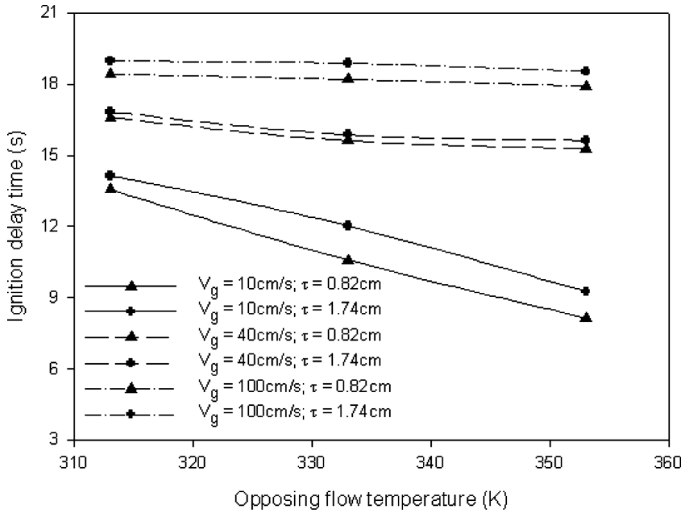

Figure 11. Ignition delay times versus opposed flow temperature at a fixed opposed flow velocity of 10 cm/s and solid fuel thicknesses of 0.82 cm and 1.74 cm.

which are consistent with the flame spread predictions described previously in Figures 5 and 9. Since the heat supplied to the solid fuel is controlled mainly by the flame temperature, the heat flux received by the solid fuel in the first regime increases rapidly due to the rapid rise of the flame temperature. However, in the second regime, the flame temperature is reduced as the flow velocity increases, reducing the heat supplied to the solid fuel. The change of heat flux in a fast flow is insignificant because the variation in the flame temperature is slight.

The effects of the opposed flow temperature and solid fuel thickness on the flame spread characteristics are also investigated in this work. Figure 11 plots the ignition delay as a function of the opposed flow temperature at three opposed flow velocities of 10 cm/s, 40 cm/s and 100 cm/s and 2 solid fuel thicknesses of 0.82 cm and 1.74 cm. Notably, both gas and solid phase radiation is considered. Figure 11 reveals that the ignition delay time decreases as the opposed flow temperature increases at a fixed opposed flow velocity regardless of whether the solid fuel thickness is 0.82 cm or 1.74 cm. This is because that the hotter opposed flow temperature preheats the solid fuel more effectively, reducing the quantity of heat needed to raise the solid surface temperature to its pyrolysis temperature. The time required to pyrolyze the fuel vapors mixed with air to form the flammable mixture is reduced. Consequently, the flame can be ignited more quickly. Furthermore, this figure shows that the variation in the ignition delay becomes negligible as the opposed

flow velocity is increased further, suggesting that the effect of the opposed flow temperature on flame ignition becomes weaker in the faster flows. Restated, the effect of the opposed flow velocity is more important than that of the opposed flow temperature, which fact was confirmed by Pan (1999), Wu et al. (2003) and Chang et al. (2006). Additionally, the ignition delay times with a solid fuel thickness of 1.74 cm are all expected to be longer than those with a solid fuel thickness of 0.82 cm. A thicker solid fuel has a greater thermal inertia which is defined as the ability of a material to conduct and store heat (Di Blasi, 1995); hence the solid fuel requires more time to receive the heat required for it to reach the pyrolysis temperature, these increasing the ignition delay time.

Figure 12 plots the flame spread rate versus the opposed flow temperature at three opposed flow velocities of 10 cm/s, 40 cm/s and 100 cm/s and two solid fuel thicknesses of 0.82 cm and 1.74 cm. As expected, a hotter opposed flow leads to a stronger flame. For example, the non-dimensional maximum flame temperatures at the opposed flow temperatures of 313 K, 333 K and 353 K are 5.286, 5.343 and 5.44, respectively, at a fixed opposed flow velocity of 40 cm/s. The enhanced pyrolysis intensity shortens the formation time of the flammable mixture ahead of the flame front. Hence, the flame spread rate increases with the flow temperature at a fixed opposed flow velocity. Note that the flame spread rate at an opposed flow velocity of 10 cm/s and a temperature of 313 K is the lowest among all opposed flow velocities. However,

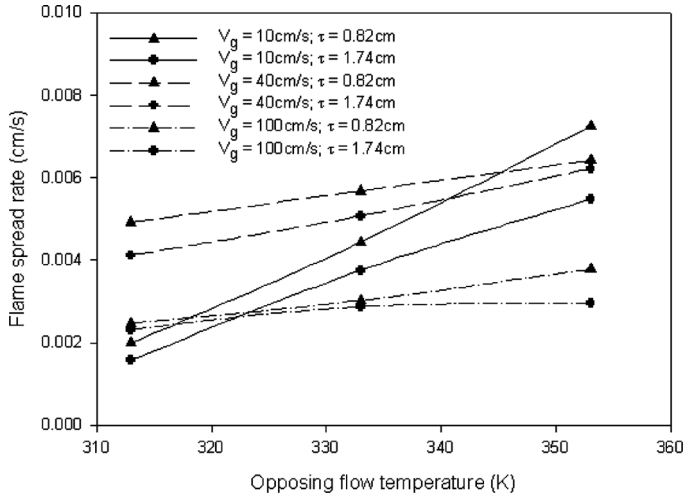

Figure 12. Flame spread rate versus opposed flow temperature at a fixed opposed flow velocity of 10 cm/s and 2 solid fuel thicknesses of 0.82 cm and 1.74 cm.

the variation of the flame spread rate at an opposed flow velocity of 10 cm/s is steepen than those at 40 and 100 cm/s as the opposed flow temperature increases, revealing that the influence of the upstream gas temperature on the flame spread rate is stronger at the lower flow speeds. Moreover, a comparison between two solid fuel thicknesses shows that the flame spread rates over the thicker solid fuel sample are all slower than those of the thinner fuel. Di Blasi (1995) and Di Blasi and Wichman (1995) also obtained this finding. As mentioned previously, this result is attributed to the fact that a thicker solid fuel has a greater thermal inertia, such that increasing the temperature of the fuel is more difficult. Accordingly, the solid fuel takes longer to form the flammable mixture near the solid fuel surface, reducing the flame spread rate.

CONCLUSIONS

This work utilizes an unsteady combustion model, with variable opposed flow velocity and temperature, solid fuel thickness and radiation effect as parameters, to investigate their effects on flame ignition and subsequent downward flame spread over a finite-length PMMA slab with mixed convection conditions in a two-dimensional wind tunnel. The previous studies mostly are addressed either thermally thick or thin materials, whereas the present work is emphasized on intermediate-thickness materials. The gas and solid phase temperatures, preheat length and the heat flux are used to examine flame ignition and spread characteristics. The numerical results show that the ignition delay time increases with the opposed flow velocity and it increases when radiation is considered. Additionally, the flame spread behaviors can be divided into two regimes based on the opposed flow velocity: one is the oxygen transport control regime and the other is the chemical kinetic control regime. The steady flame spread rate firstly increases and then declines as the opposed flow velocity is increased continuously. Furthermore, the results demonstrate that radiation weakens the flame and always reduces the corresponding spread rate. When compared with the radiation heat loss from the solid to the ambient, the gas phase radiation feedback is insignificant and can be neglected. This work also discusses the influences of the opposed flow temperature and solid fuel thickness on the flame spread behavior. The predictions indicate that the hotter opposed flow temperature facilitates ignition and enhances the flame strength as defined by an increase in the corresponding spread rate. The ignition delay time becomes longer and the flame spread rate is reduced as the solid fuel thickness is increased. The comparison of ignition delay time and flame spread rate between several opposed flow velocities and temperatures demonstrates that the influence of the opposed flow temperature on the flame becomes

inconspicuous as the opposed flow velocity is increased further. All of these results should be of assistance and guidance to the development of the models that seek to incorporate additional physical processes.

NOMENCLATURE

a	Gas phase velocity gradient
$\overline{C}_p$	Specific heat for gas mixture, J/g K
$\overline{H}$	Height of the wind tunnel
$\overline{I}_b$	blackbody intensity
$\bar{k}$	Conductivity, W/cm K
$\bar{q}$	Heat of combustion per unit mass of fuel, J/g
$\bar{q}_{gr}$	Gas phase radiation heat flux, W/cm^2
$\bar{q}_{sr}$	Solid phase radiation heat flux, W/cm^2
$\bar{t}$	Time, s
$\overline{T}$	Gas phase temperature, K
$\overline{T}_s$	Solid phase temperature, K
$\bar{u}$	Velocity parallel to the fuel surface, cm/s
$\bar{v}$	Velocity normal to the fuel surface, cm/s
$\overline{V_g}$	opposed flow velocity
$\bar{x}$	Coordinate parallel to the fuel surface, cm
$\bar{y}$	Coordinate normal to the fuel surface, cm

Greek Symbols

$\bar{\alpha}$	Thermal diffusivity, cm^2/s
$\bar{\rho}$	Density of gas phase, g/cm^3
$\bar{\tau}$	Solid fuel thickness, cm
ε	Surface emissivity
$\dot{\omega}_F$	Non-dimensional gas phase reaction rate

Overhead

-	Dimensional quantities

Subscript

s	Solid phase
∞	Ambient condition

REFERENCES

Aynai, M.B., Esfahani, J.A., and Mehrabian, R. (2006) Downward flame spread over PMMA sheets in quiescent air: Experimental and theoretical studies. *Fire Saf. J.*, **41**, 164.

Bhattacharjee, S. and Altenkirch, R.A. (1991) The effect of radiation on flame spread in a quiescent, microgravity environment. *Combust. Flame*, **84**, 160.

Bhattacharjee, S., King, M., Takahashi, S., Nagumo, T., and Wakai, K. (2000) Downward flame spread over poly(methyl)methacrylate. *Proc. Combust. Inst.*, **28**, 2891.

Chang, W.K., Chen, C.H., and Liou, T.M. (2006) Numerical study for downward flame spread over a finite-length PMMA with radiation effect. *International Journal of Transport Phenomena*, in press.

Chen, R.J. (1999) Experimental Analyses of Flame Spread Behavior Over Solid Fuel Under Suddenly Opposed Flow, MS thesis, National Tsing Hua University, Hsinchu, Taiwan, R.O.C.

Delichatsios, M.A. (1986) Exact solution for the rate of creeping flame spread over thermally thin materials. *Combust. Sci. Technol.*, **44**, 257.

DeRis, J.N. (1968) The Spread of a Diffusion Flame over a Combustible Surface, Ph. D. Thesis, Harvard University.

Di Blasi, C. (1995) The influences of sample thickness on the early transient stages of concurrent flame spread and solid burning. *Fire Saf. J.*, **25**, 287.

Di Blasi, C. and Wichman, I.S. (1995) Effect of solid-phase properties on flames spreading over composite materials. *Combust. Flame*, **102**, 229.

Fernandez-Pello, A.C. and Hirano, S.T. (1982) Controlling mechanisms of flame spread. *Combust. Sci. Technol.*, **32**, 1.

Fujita, O., Nishizawa, K., and Ito, K. (2002) Effect of low external flow on flame spread over polyethylene insulated wire in microgravity. *Proc. Combust. Inst.*, **29**, 2545.

Grosshandler, W.L. (1993) RADCAL: A Narrow-Band Model for Radiation Calculations in a Combustion Environment, *NIST Technical Note 1402*.

Higuera, F.J., Linan, A., and Iglesias, I. (1997) Effects of boundary layer displacement and separation on opposed-flow spread. *Combust. Theory Modeling*, **1**, 65.

Lin, P.H. and Chen, C.H. (2000) Numerical analyses for radiative autoignition and transition to flame spread over a vertically oriented solid fuel in a gravitational field. *Combust. Sci. Technol.*, **151**, 157.

Olson, S.L. (1991) Mechanisms of microgravity flame spread over a thin solid fuel: Oxygen and opposed flow effects. *Combust. Sci. Technol.*, **76**, 233.

Pan, I.J. (1999) Experimental Analyses of Flame Spread Behavior Over Solid Fuel Under Opposed Flow, MS thesis, National Tsing Hua University, Hsinchu, Taiwan, R. O. C.

Patankar, S.V. (1980) Numerical Heat Transfer and Fluid Flow, McGraw-Hill, New York.

Rhatigan, J.L., Bedir, H., and T'ien J.S. (1998) Gas-phase radiative effects on the burning and extinction of a solid fuel. *Combust. Flame*, **112**, 231.

Siegel, R. and Howell, J.R. (1992) Thermal Radiation Heat Transfer, McGraw-Hill, Washington, DC.

Son, Y. and Ronney, P.D. (2002) Radiation-driven flame spread over thermally thick fuels in quiescent microgravity environment. *Proc. Combust. Inst.*, **29**, 2587.

Takahashi, S., Nagumo, T., Wakai, K., and Bhattacharjee, S. (2000) Effect of ambient condition on flame spread over a thin PMMA sheet. *JSME Int. J. Ser. B-Fluids Therm. Eng.*, **43**, 556.

Takahashi, S., Kondou, M., Wakai, K., and Bhattacharjee, S. (2002) Effect of radiation on flame spread over a thin PMMA sheet in microgravity. *Proc. Combust. Inst.*, **29**, 2579.

Tizon, J.M., Salva, J.J., and Linan, A. (1999) Wind-aided flame spread under oblique forced flow. *Combust. Flame*, **119**, 41.

Wichman, I.S. and Williams, F.A. (1983a) Simplified model of flame spread in an opposed flow along a flat surface of a semi-infinite solid. *Combust. Sci. Technol.*, **32**, 91.

Wichman, I.S. and Williams, F.A. (1983b) Comments on rates of creeping spread of flame over thermally thin fuels. *Combust. Sci. Technol.*, **33**, 207.

Wichman, I.S. (1992) Theory of opposed-flow flame spread. *Prog. Energy Combust. Sci.*, **18**, 553.

Wichman, I.S. and Osman, A.M. (1998) Flame spread over a flat, combustible, thermally thick solid in an opposed oxidizer shear flow. *Combust. Flame*, **112**, 623.

Wu, K.K., Fan, W.F., Chen C.H., Liou, T.M., and Pan, I.J. (2003) Downward flame spread over a thick PMMA slab in an opposed flow environment: Experiment and modeling. *Combust. Flame*, **132**, 697.

Wu, K.K. and Chen, C.H. (2004) Radiation effects for downward flame spread over a thermally thin fuel in a partial gravity environment. *Combust. Sci. Technol.*, **176**, 1909.

West, J., Bhattacharjee, S., and Altenkirch, R.A. (1994) Surface radiation effects on flame spread over thermally thick fuels in an opposing flow. *J. Heat Transf.-Trans. ASME*, **116**, 646.

Wichman, I.S. (1983) Flame spread in an opposed flow with a linear velocity gradient. *Combust. Flame*, **50**, 287.

Zhu, X.L. and Gore, J.P. (2005) Radiation effects on combustion and pollutant emissions of high-pressure opposed flow methane/air diffusion flames. *Combust. Flame*, **141**, 118.